A COMPARISON OF CO-CURRENT AND COUNTER-CURRENT MODES FOR FISCHER TROPSCH SYNTHESIS IN TWO CONSECUTIVE REACTOR OF OXIDATIVE COUPLING OF METHANE AND FISCHER TROPSCH

Abbas Ghareghashi[1], Sattar Ghader[*1,2], Hassan Hashemipour[1], Hamed Rashidi Moghadam[3]

[1]Department of Chemical Engineering, College of Engineering, Shahid Bahonar University of Kerman, Jomhoori blvd., Kerman, Iran.

[2]Minerals Industries Research Center, Shahid Bahonar University of Kerman, Kerman, Iran

[3]Department of Chemical and Petroleum Engineering, Sharif University of Technology, Tehran, Iran.

ABSTRACT

The results of three cases of two consecutive reactors are studied in two types of co-current and counter-current flow in second reactor where two consecutive reactors are oxidative coupling of methane (OCM) and Fischer-Tropsch (FT) reactors. FT reactor can be fixed bed or membrane fixed bed reactor with a hydrogen perm-selective membrane. Effect of CH_4/O_2 ratio, contact time, inlet temperature, and amount of N_2 in OCM feed on C_2 to C_{5+} hydrocarbons produced in FT reactor were studied. Results show that use of counter-current hydrogen-perm selective membrane FT reactor that sequenced after OCM reactor improves the C_{5+} yield as a desirable product and reduces the amount of CH_4 and CO_2 as by products of FT reactor in comparison to co-current and conventional reactor. This phenomenon can be explained with more H_2 diffusion through the membrane and more CO conversion and more hydrocarbons productions, briefly.

Keywords: Fischer–Tropsch, oxidative coupling of methane, C_{5+} yield, membrane reactor, counter-current, CH_4 yield, CO_2 yield

1. INTRODUCTION

A great part of the world energy source is liquid hydrocarbons such as gasoline, diesel and etc. In recent decays, liquid hydrocarbon fuels synthesized from natural gas has become interesting. The Fischer-Tropsch (FT) process is a good method for hydrocarbon production and can be used instead of liquid hydrocarbons that are produced from crude oil. This substitution has many advantages such as making low sulfurous fuel and no variation of these fuels price with crude oil price that is high in recent years. The FT process converts hydrogen and carbon monoxide (syngas) to liquid hydrocarbons. Coal, natural gas and biomass can be source of syngas. Main reaction of FT process is:

$$(2n + 1)\ H_2 + n\ CO \rightarrow C_nH_{(2n+2)} + n\ \underline{H_2O} \quad (1)$$

Here *n* is a positive integer that shows the number of carbon atoms in hydrocarbon product.

Variable grades of synthetic hydrocarbon fuels (e.g., gasoline; C_5–C_{12}, diesel; C_{13}–C_{18}, soft wax; C_{19}–C_{23}, medium wax; C_{24}–C_{35}, hard wax; C_{35+}) can be produced depending on temperature, pressure and catalyst used in FT process [1]. C_{5+} fuel is more favorable because of its higher price and demand. C_{5+} that obtained from FT process mainly consists of n-paraffin and leads to lower octane number compared to crude oil C_{5+}. Bifunctional catalysts promote yield and octane number of FT C_{5+} [2].

FT reaction has side reactions that decrease the yield of hydrocarbon fuels. Most important side reaction is water gas shift reaction:

$$H_2O + CO \rightarrow H_2 + CO_2 \quad (3)$$

and, second side reaction is reverse of steam reforming reaction:

$$CO + 3\,H_2 \rightarrow H_2O + CH_4 \quad (4)$$

Many investigations have been done to increase the gasoline production and decrease the CH_4 and CO_2 formation during this FT process. Synthesizing new catalysts and modification of synthesized catalysts and changing the structure of FT reaction reactor are the main efforts in this way. Using hydrogen perm-selective membrane fix bed and fluidized bed reactors are one of the major ways to increase C_{5+} and decrease major by-products. Silvano et al. [3] classified catalytic membrane reactors according to the type of membrane (perm-selective/non perm-selective) and the location of the catalyst (within/outside the membrane). Also, Rohde and Unruh [4] proposed four concepts to use membrane reactors in Fischer-Tropsch synthesis (FTS): distributed feed of reactants, in situ removal of water, forced through membrane contactor and zeolite encapsulated catalysts. Forghani et al. [5] showed that by using hydrogen perm-selective membrane reactor the yield of gasoline fuel must be increased. Rahimpour et al. [6, 7, 8] used many types of membrane reactor like: H_2 perm selective and H_2O removal membrane reactor in co-current and counter-current modes. They mentioned that this reactor resulted in higher CO and H_2 conversion and gasoline production. Using hydrogen selective membrane in the FT reactor improves the reaction's yield and selectivity by shifting the thermodynamic equilibrium and increasing the reactants conversion. [9]. Silver alloyed palladium has very good permeability of hydrogen [10, 11].

Syngas is the feed of FT process. However, the product of oxidative coupling of methane (OCM) process can also be fed to FT process to convert syngas to high value hydrocarbons, because OCM products contain large amount of H_2 and CO as by product. The OCM is a straight method to upgrade natural gas and convert methane to C_{2+}, but, it has low selectivity and low yield [12]. Various types of reactors with various configuration and operational condition have been used to improve the yield of ethylene production in OCM reaction [13, 14].

In this paper, OCM and FT reactors were used consecutively. In FT reactor two cases of counter-current and co-current flow of OCM exiting gas are discussed. FT reactor was equipped with hydrogen perm-selective membrane reactor with Pd-Ag membrane in one case. We discuss the amount of C_{5+} as desirable product in different conditions of FT reactor. Moreover, in this article we discuss yield of CO_2 and CH_4 as by products in each condition. According to observed results, counter current flow in FT reactor causes more yield of C_{5+} and lower CO_2 and CH_4 yield than co-current flow.

2. Process description

As will be described in the later sections, methane is converted to heavy hydrocarbons in two reactors. The OCM reactor is first one in which synthesis gas and C_{2+} is produced for second reactor where it converts CO and H_2 to heavy hydrocarbons. In an extra configuration, second reactor is equipped with a membrane with high selectivity to hydrogen allowing continuous adding of hydrogen to FT reaction medium. OCM reactor is a fixed bed reactor packed with La_2O_3/CaO catalyst operated at total pressure of 110 kPa. Oxygen, methane and nitrogen as a dilute gas were fed to OCM reactor and the products that contain C_{2+} and syngas were fed to FT reactor. Research Institute of Petroleum Industry (RIPI) in Iran has demonstrated a pilot plant for FT synthesis with a 12 m water cooled fixed bed reactor [15]. The operational conditions of FT reactor are listed in Table 1. FT reactor has a length of 12 m and a diameter of 0.0381. The

FT membrane reactor is a shell and tube configuration where bifunctional Fe-HZSM5 catalyst (metal part: 100 Fe/5.4 Cu/7K_2O/21SiO_2, acidic part: SiO_2/ Al_2O_3 528) was packed in tubes. The membrane of FT reactor was between tube and shell and was perm-selective to hydrogen that allows hydrogen to diffuse to shell with hydrogen partial pressure gradient. This permeation makes heat and mass transfer possible that causes higher hydrocarbon fuel production. Flow of OCM gas flow in FT membrane reactor can be co-current and counter-current. Counter-current flow provides higher mass and heat gradient that may improve hydrocarbon fuel yield. The operational conditions of OCM reactor are shown in Table 2. The operational condition of membrane FT reactor is summarized in Table 3. Schematic of two consecutive conventional FT reactor (fixed bed) with OCM reactor is shown in Fig 1. Total schematic of this process and detailed schematic of fixed bed membrane FT reactor for co-current and counter-current flow are shown in Figs. 2 and 3, respectively. It is assumed that a heat exchanger decreases OCM reactor product temperature to FT reactor feed temperature.

3. Model equations

3.1. OCM reactor

3.1.1. OCM kinetics modeling

Kinetic modelling of OCM reaction over La_2O_3/CaO catalyst has been reported by Stanch et al. [16]. This model contains nine catalytic reactions and one gas phase reaction which are listed below. First three reactions are methane oxidation reaction. Reaction 5 and 6 are C_{2+} oxidation reaction. Reaction 4 is carbon monoxide oxidation. Reactions 8 to 10 are side reactions.

$$\text{Step 1}: \ CH_4 + 2O_2 \rightarrow CO_2 + 2H_2O \tag{5}$$

$$\text{Step 2}: \ 2CH_4 + 0.5O_2 \rightarrow C_2H_6 + H_2O \tag{6}$$

$$\text{Step 3}: \ CH_4 + O_2 \rightarrow CO + H_2O + H_2 \tag{7}$$

$$\text{Step 4}: \ CO + 0.5O_2 \rightarrow CO_2 \tag{8}$$

$$\text{Step 5}: \ C_2H_6 + 0.5O_2 \rightarrow C_2H_4 + H_2O \tag{9}$$

$$\text{Step 6}: \ C_2H_4 + 2O_2 \rightarrow 2CO + 2H_2O \tag{10}$$

$$\text{Step 7}: \ C_2H_6 \rightarrow C_2H_4 + H_2 \tag{11}$$

$$\text{Step 8}: \ C_2H_4 + 2H_2O \rightarrow 2CO + 4H_2 \tag{12}$$

$$\text{Step 9}: \ CO + H_2O \rightarrow CO_2 + H_2 \tag{13}$$

$$\text{Step 10}: \ CO_2 + H_2 \rightarrow CO + H_2O \tag{14}$$

The reaction rates for each step are given below:

$$r_j = \frac{(k_{0,j} e^{-E_{a,j}/RT} P_C^{m_j} P_{O_2}^{n_j})}{(1 + K_{j,co_2} e^{-\Delta H_{ad,co_{2,j}}/RT} P_{CO_2})^2} \qquad j = 1, 3-6 \tag{15}$$

$$r_2 = \frac{k_{0,2} e^{-E_{a,2}/RT} (K_{0,o_2} e^{-\Delta H_{ad,o_{2,j}}/RT} P_{O_2})^{n_2} P_{CH_4}}{[1 + (K_{0,o_2} e^{-\Delta H_{ad,o_{2,j}}/RT} P_{O_2})^n + K_{j,co_2} e^{-\Delta H_{ad,co_{2,j}}/RT} P_{CO_2}]^2} \tag{16}$$

$$r_7 = k_{0,7} e^{-E_{a,7}/RT} P_{C_2H_6} \tag{17}$$

$$r_8 = k_{0,8} e^{-E_{a,8}/RT} P_{C_2H_6}^{m_8} P_{H_2O}^{n_8} \quad (18)$$

$$r_9 = k_{0,9} e^{-E_{a,9}/RT} P_{CO}^{m_9} P_{H_2O}^{n_9} \quad (19)$$

$$r_{10} = k_{0,10} e^{-E_{a,10}/RT} P_{CO_2}^{m_{10}} P_{H_2}^{n_{10}} \quad (20)$$

The kinetic parameters used for the above reaction scheme are presented in Table 4.

3.3.2. OCM reactor mathematical model

For mathematical modeling of OCM reactor one dimensional steady state plug flow reactor was assumed. It was assumed that the gas phase in reactor is ideal gas. According to these assumptions we can write following mass and energy balance equations:

Mass balance:

$$-u_s \frac{dC_j}{dz} - \rho_b r_{c,j} + \varepsilon_b r_{g.j} = 0 \quad (21)$$

Energy balance:

$$-u_s \rho_g \sum c_p \frac{dT}{dz} + \rho_b \sum r_i \left(-\Delta H\right)_i + \varepsilon_b \sum r_i \left(-\Delta H\right)_i - 4\frac{U}{d_t}\left(T - T_{ex}\right) = 0 \quad (22)$$

Momentum balance (Ergun's equation):

$$-\frac{\mathrm{d}P}{\mathrm{d}z} = \frac{\rho_g u_s^2}{\psi d_p}\left(\frac{1-\varepsilon}{\varepsilon^3}\right)\left[\frac{150\left(1-\varepsilon\right)}{\psi\ \mathrm{Re}} + 1.75\right] \quad (23)$$

3.2. FT reactor

3.2.1. FT kinetics modeling

FT reactions are given by Rahmati and Soleimani [17] :

$$\text{Step 1}: CO + 3H_2 \xrightarrow{R_1} CH_4 + H_2O \quad (24)$$

$$\text{Step 2}: 2CO + 4H_2 \xrightarrow{R_2} C_2H_4 + 2H_2O \quad (25)$$

$$\text{Step 3}: 2CO + 5H_2 \xrightarrow{R_3} C_2H_6 + 2H_2O \quad (26)$$

$$\text{Step 4}: 3CO + 7H_2 \xrightarrow{R_4} C_3H_8 + 3H_2O \quad (27)$$

$$\text{Step 5}: 4CO + 9H_2 \xrightarrow{R_5} n - C_4H_{10} + 4H_2O \quad (28)$$

$$\text{Step 6}: 4CO + 9H_2 \xrightarrow{R_6} i - C_4H_{10} + 4H_2O \quad (29)$$

$$\text{Step 7}: 6.05CO + 12.23H_2 \xrightarrow{R_7} C_{6.05}H_{12.36}(C_5^+) + 6.05H_2O \quad (30)$$

$$\text{Step 8}: CO + H_2O \xleftrightarrow{R_8} CO_2 + H_2O \quad (31)$$

The reaction rate equations of each reaction step are given below:

$$R_i = 0.278 K_i \exp\left(\frac{-E_i}{RT}\right) P_{co}{}^{m} P_{H_2}^{n} \tag{32}$$

The kinetic parameters of each reaction are listed in Table 5. These parameters are for temperature between 290 to 310 °C; pressure between 15 to 23 bars and H_2/CO ratio between 0.76–1.8 [17]. The desirable reaction is reaction 7.

3.2.2. FT reactor mathematical model

The FT reactor was assumed one dimensional plug flow reactor. It was assumed that the gas phase in this part of reactor is ideal gas. On above assumptions, the mass and energy balance equations can be written:

Mass balance in gas phase:

$$\frac{-F_t}{A_c}\frac{dy_i}{dz} + a_v c_t k_{gi}\left(y_{is} - y_i\right) = 0 \tag{33}$$

Mass balance in solid phase:

$$a_v c_t k_{gi}\left(y_i - y_{is}\right) + \rho_b \eta r_i = 0 \qquad i = 1, 2, \ldots, N-1 \tag{34}$$

Energy balance in gas phase:

$$\frac{-F_t}{A_c} C_{pg}\frac{dT}{dz} + a_v h_f\left(T_s - T\right) + \frac{\pi D_i}{A_c} U_{shell}\left(T_{shell} - T\right) = 0 \tag{35}$$

Energy balance in solid phase:

$$a_v h_f\left(T - T_s\right) + \rho_b \eta \sum r_i\left(-\Delta H_i\right) = 0 \tag{36}$$

Where, y_i, T, y and T_s are the mole fraction and temperature in gas phase and mole fractions on the catalyst surface and solid phase temperature, respectively.

3.2.3. Membrane fixed bed mathematical model

3.2.3.1. Shell side (reaction side)

In the shell side of this reactor FT reaction occurs and the assumptions are the same as fixed bed FT reactor. On the basis of those assumptions, the balance equations can be written as:

Mass balance in gas phase:

$$\frac{F_t}{A_{shell}}\frac{dy_i}{dz} = \frac{\alpha_H}{A_s}\left(\sqrt{P_H^t} - \sqrt{P_H^{sh}}\right) + a_v c_t k_{gi}\left(y_{is} - y_i\right) \tag{37}$$

Mass balance in solid phase:

$$a_v c_t k_{gi}\left(y_{is} - y_i\right) = \eta r_i \rho_b \qquad i = 1, 2, \ldots, N-1 \tag{38}$$

Energy balance in gas phase:

$$\frac{F_t}{A_c}C_{pg}\frac{dT}{dz}=\frac{\pi D_{ro}}{A_{shell}}U_{shell}\left(T_{shell}-T\right)+\frac{\pi D_i}{A_c}U_{tube}\times\left(T_{tube}-T\right)+\frac{\alpha_H}{A_s}\left(\sqrt{P_H^t}-\sqrt{P_H^{sh}}\right)C_{ph}$$
$$\times\left(T_{tube}-T\right)+a_v h_f\left(T_s-T_i\right) \quad (39)$$

Energy balance in solid phase:

$$a_v h_f\left(T_s-T\right)=\rho_b\eta\sum r_i\left(-\Delta H_i\right) \quad (40)$$

Where F_t is total molar flow rate of gas in reaction side. D_i and D_{ro} are the inner and outer diameter of tube side, respectively. ρ_b is bed density and P_H^{sh} and P_H^t are partial pressures of hydrogen in shell and tube sides. ΔH_i is enthalpy of reaction *i*. In addition, α_H is hydrogen permeation rate constant defined below [18, 19, 20]:

$$\alpha_H=\frac{2\pi LP_0\exp\left(-E_P/RT\right)}{\ln(R_o/R_i)} \quad (41)$$

Where R_o and R_i are outer and inner radius of Pd-Ag layer. P_0 factor above 200^0C is reported as $6.33\times10^{-8}\left(molm^{-2}s^{-1}pa^{-1/2}\right)$ and activation energy E_p is 15.7 kJ/mol [42, 43].

3.2.3.2. Tube side (OCM gas flow side)

Mass and energy balance equations in tube side are:

Mass balance:

$$\pm\frac{1}{A_c}\frac{dF_i^t}{dz}=\frac{\alpha_H}{A_s}\left(\sqrt{P_H^t}-\sqrt{P_H^{sh}}\right) \quad (42)$$

Energy balance:

$$\pm\frac{F_t}{A_c}C_{pg}\frac{dT_{tube}}{dz}=\frac{\pi D_i U_{tube}}{A_c}\left(T_{tube}-T\right)+\frac{\alpha_H C_{ph}}{A_s}\times\left(\sqrt{P_H^t}-\sqrt{P_H^{sh}}\right)\left(T_{tube}-T\right) \quad (43)$$

In equation (42) and (43) + refers to co-current flow and – refers to counter-current flow in membrane fixed bed FT reactor.

4. Numerical solution

All of these simulations were solved by numerical analysis. The initial conditions at the entrance of the OCM reactor at z=0 are:

$C_n = C_n^0$, $C_m = C_m^0$, $T = T^0$, and $P = P^0$

Where *n* represents reactants and inert in feed, and *m* represents products.

The boundary conditions for the bulk phase in conventional fixed bed FT reactor and in shell side of membrane fixed bed reactor at $z=z_1$ are:

$$y_i = y_{i,in} \quad , \quad T = T_{in}$$

The boundary conditions of tube side of membrane fixed bed FT reactor that OCM gas flows in at z = z_1 in co-current flow and in z=z_2 in counter-current flow are:

$$y_i = y_{i,f} \quad , \quad T = T_f$$

Where y_i and T_f are the mole fraction of component *i* and temperature of feed stream, respectively. z_1 and z_2 are the beginning start and end of fixed bed membrane FT reactor, respectively. The reactor performance is expressed by conversion of reactants and yield of products.

5. Results and discussion

The effect of CH_4 to O_2 ratio in OCM reactor feed on CO and H_2 conversion and yield of each hydrocarbon was studied. The variation of each hydrocarbon flow and yield was also included in each case of FT reactor. The amount of CH_4 and CO_2 as a byproduct of FT reactor were also studied in each case of reactor.

5.1. Validation of reactors model

Both of FT and OCM modeling must be validated before theoretical analysis. OCM reactor model was validated by comparing its calculation results with experimental results of Stansch [16]. FT reactor was validated by comparison its model data with experimental data of RIPI pilot plant [15]. Both of these models show good fit to the experimental data and as Tables 6 and 7 show the agreements between OCM and FT reactor with experimental data is good.

5.2. Effect of CH_4/O_2 ratio in OCM feed

Fig 4 shows that with increasing of CH_4/O_2 ratio, H_2/CO ratio is decreased because CO produces more with increasing of CH_4 amount in OCM reactor feed. This phenomenon can be explained by the OCM kinetic equations of Snatch [16]. Reaction 10 proceeds more because of increasing in amount of H_2 and CO produced.

The figure begins from CH_4/O_2=2, because all hydrocarbons are oxidized to CO_2 for CH_4/O_2<2. According to Fig. 4, when CH_4/O_2 ratio increases, the amount of CO increases and CO cannot be completely consumed and H_2 conversion also decreases when CO conversion decreases. As shown in Fig 5 in counter-current flow in membrane reactor (COUN-MR) the gradient of H_2 among two side of membrane increases and more H_2 can diffuse through membrane which leads to more CO conversion and lower H_2 conversion because amount of H_2 in reaction side of membrane reactor increases. COUN-MR, CO-MR and CR refer to countercurrent, co-current and conventional reactor. In Fig. 6 partial pressure of hydrogen and its diffusion rate through membrane in two counter-current and co-current flow are shown. Fig. 6 explains more H_2 diffusion rate through membrane in COUN-MR in comparison to CO-MR (co-current membrane reactor). Rate of hydrogen permeation is very high at beginning of reactor for COUN-MR because of very high pressure difference. Pressure gradient for COUN-MR decreases and for CO-MR increases through length of reactor.

Fig 7 shows that when CH_4/O_2 ratio increases, the amount of oxygen in OCM reactor decreases and this lead to lower yield of C_2 products. In other words, when O_2 amount increases in feed the selectivity of C_2 products (between C_2H_6 and C_2H_4) decreases. Reaction order is negative for C_2H_6 and positive for C_2H_4 in

FT kinetics expressed by Rahmati et al [17]. According to increasing CO amount with increasing CH_4/O_2 ratio, C_2H_4 yield increases and C_2H_6 yield decrease.

The yield of C_{5+} increases with increasing CH_4/O_2 ratio as shown in Fig 8, because amount of CO in FT reactor increases. When COUN-MR is used more H_2 is present in reaction side of membrane reactor and this leads to more C_{5+} production and more yield.

As Fig. 9 shows, with increasing CH_4/O_2 ratio and more CO production, the yield of CH_4 decreases and yield of CO_2 increases due to their reaction order in FT kinetics. But yield of both of them decrease in COUN-MR in comparison to CO-MR and conventional reactor (CR) and it is favorable.

5.3.2. Effect of N_2 percentage in OCM feed as an inert gas

As shown in Fig. 10 H_2/CO ratio is decreased in OCM reactor until 60 % N_2 in feed and then increases. N_2 as an inert gas influences both of reactors. In OCM reactor, N_2 reduces the temperature of reaction with absorbing heat of reaction. In all figures that show the effect of inert gas a maximum or minimum point can be observed. Fig. 11 shows the effect of COUN-MR on H_2 conversion that is lower than CO-MR because more H_2 diffuses through membrane. When inert gas used in syngas if partial pressure of CO and H_2 are constant nitrogen does not affect reaction kinetics [21, 22]. But as shown Fig 11 with increasing of N_2 in FT reactor and decreasing partial pressure of CO and H_2 both of conversions decrease until inert gas percentage about 60% and then increases and this is the effect of heat absorbing by inert gas in system.

When inert gas is low in OCM reactor, higher reaction temperature would be achieved. This result moves forward dehydrogenation of ethane to ethylene. But with increasing amount of inert gas this reaction becomes not significant and more C_2H_6 is produced as shown in Fig 12. In Fig. 13 more C_{5+} yield are obtained in COUN-MR reactor because of increasing amount of H_2 in reaction side of membrane reactor.

Fig 14 shows the effect of inert gas on byproducts of FT reaction which is decreasing the amount of CH_4 and increasing amount of CO_2. This trend was also observed in Fig 9 that shows the effect of CH_4/O_2 ratio on byproducts. Both effects on CO_2 and CH_4 yields shown in Figs. 9 and 14 can be explained by FT kinetic equation. As a conclusion, increasing the amount of N_2 as an inert gas to about 60 % of total feed has favorable effect on desirable products.

5.3.3. Components mole flow and products yield in reactors

Figs. 15 and 16 show the molar flow of CO and H_2 in OCM and FT reactor. Figs 15(b) and 16(b) show molar flow of H_2 and CO at end of FT reactor. As expected, the COUNT-MR molar flow of CO is lower and H_2 is more than CR and CO-MR, because more H_2 is present in reaction side of membrane reactor and more CO is consumed. Figs. 17 and 18 show the molar flow rate of C_2H_6 and C_2H_4 in two consequent reactors.

In Figs. 19 to 22 increase of molar flow and yield of C_3 to C_{5+} hydrocarbons in COUN-MR mode is observed compared to CO-MR and CR because more H_2 permeates through membrane and reaction of C_3 to C_{5+} hydrocarbons proceed more and desirable product formation will be more. The amount of byproducts increases along the reactor length as shown in Fig. 23 but this amount is less for COUN-MR.

5.3.4. Effect of OCM inlet temperature

Effect of OCM reactor inlet temperature on C_{5+} yield is shown in Fig. 24. In this Figure C5+ yield is shown as a function of CH_4/O_2 ratio, N_2 percentage in feed of OCM reactor and length of FT reactor. Higher temperature provides more C_{5+} yield in all three types of FT reactor modes of operation.

Fig 25 shows gas phase temperature in OCM reactor and FT reactor in all three modes of operation. As shown in Fig 25 gas phase temperature of OCM reactor is increased along the OCM reactor length. However, in the case of FT reactor temperature increases sharply at the beginning of CR reactor and then decreases. But in membrane FT reactor because of heat transfer between two sides of reactor the sharp increase of temperature is not observed which is useful for reactor processing.

5.3.5. Effect of contact time

As shown in Fig. 26 with increasing contact time in OCM reactor, the H_2/CO ratio in OCM reactor decreases and this lead to more conversion in FT reactor due to more CO presents in FT reactor. Increasing contact time has insignificant effect on C_{5+} yield. However, reactants would have longer contact time with lower space velocity which gives a little more favorable C_{5+} production.

6. CONCLUSION

Methane could be converted to useful hydrocarbons by two consecutive reactors. The flow of OCM gas in second reactor can be co-current or counter current. Furthermore, CH_4 is converted to C_{5+} by use of two reactors in series. Amount of desired components yield in membrane FT reactor is higher than conventional FT reactor due to diffusing hydrogen to the reaction side and increasing the conversion of CO in reaction side. With counter-current flow membrane reactor yield of C_{5+} as a desirable product improves more duo to more H_2 permeation through membrane and more CO conversion is achieved. By use of membrane FT reactor CH_4 and CO_2 as byproducts of FT reaction are decreased. Therefore, this reactor configuration especially counter-current flow can be suggested to produce more desirable liquid hydrocarbon fuels at the same conditions compared to conventional reactor.

SYMBOLS

A_c	Cross section area of tube (m^2)
A_{shell}	Cross section area of shell (m^2)
a_v	Specific surface area of catalyst pellet (m2.m-3)
c_p	Specific heat ($kJ.mol^{-1}.K$)
C_t	Total concentration ($mol.m^{-3}$)
C_j	concentration of species j (mol.m–3)
c_{Ph}	Specific heat of the hydrogen at constant pressure ($Jmol^{-1}K^{-1}$)
d_t	tube diameter (m)
d_p	pellet diameter (m)
D_i	Tube inside diameter (m)

D_{ro} reaction outside diameter (m)

F_t Total molar rate for shell side (mol.s^{-1})

h_f Gas-catalyst heat transfer coefficient (W.m^{-2} .K $^{-1}$)

ΔH_{rij} heat of reaction (kJmol^{-1})

k_{gi} Mass transfer coefficient between gas and solid phase for component i (m.s^{-1})

p_H^{sh} Shell side pressure (bar)

p_H^t Tube side pressure (bar)

$\overline{P}$ Permeability of hydrogen through Pd-Ag layer (mol m^{-1} s^{-1} pa$^{-1/2}$)

r_i rate of reaction i (mol g^{-1} s)

R_i inner radius of Pd-Ag layer (m)

R_o outer radius of Pd-Ag layer (m)

Re Reynolds number

T temperature (K)

T_{ex} external temperature (K)

T_{shell} Temperature of coolant stream, in fixed-bed reactor (K)

u_s superficial velocity (ms^{-1})

U Overall heat transfer coefficient (Wm^{-2} K)

U_{shell} Overall heat transfer coefficient between coolant and process streams (W.m^{-2}. K^{-1})

Greek letters

ε_b catalyst bed porosity

ρ_b density of catalyst bed (g.m^{-3})

ρ_g gas density (kgm^{-3})

α_H Hydrogen permeation rate constant (mol m^{-1} s^{-1} Pa$^{-0.5}$)

Ψ shape factor

REFERENCES

1. Dry, M. E., 1999. The Fischer-Tropsch process - commercial aspects. Catal. Today 6, 183-206.

2. Cagnoli M. V., Gallegos N. G., Alvarez A. M., Bengoa J. F., Yeramián A. A., Schmal S. G., 2002. Catalytic CO hydrogenation on potassic Fe/zeolite LTL. Appl. Catal. A.: Gen. 230, 169-175.

3. Tosti, S., Basile, A., Bettinali, L., Borgognoni, F., Gallucci, F., Rizzello, C., 2008. Design and process study of Pd membrane reactors. Int. J. Hydrogen Energy 33, 5098-5105.

4. Rohde, P. R., Unruh, D., Schaub, G., 2005. Membrane application in Fischer–Tropsch synthesis reactors—Overview of concepts. Catal Today 106, 143-148.

5. Forghani, A. A, Elekaei, H., Rahimpour, M. R., 2009. Enhancement of gasoline production in a novel hydrogen-permselective membrane reactor in Fischer–Tropsch synthesis of GTL technology. Int. J. Hydrogen Energy 34, 3965-3976.

6. Rahimpour, M. R., Elekaei, H., 2009. A comparative study of combination of Fischer–Tropsch synthesis reactors with hydrogen-permselective membrane in GTL technology. Fuel Process. Tech. 90, 747-761.

7. Rahimpour, M. R., Forghani, A. A., Khosravanipour Mostafazadeh, A., Shariati, A., 2009. A comparison of co-current and counter-current modes of operation for a novel hydrogen-permselective membrane dual-type FTS reactor in GTL technology. Fuel Process. Tech., 91, 33–44.

8. Rahimpour, M. R., Elekaei, H., 2009. Optimization of a novel combination of fixed and fluidized-bed hydrogen-permselective membrane reactors for Fischer–Tropsch synthesis in GTL technology. Chem. Eng. J., 152, 543-555.

9. Sanchez, J., Tsotsis, T. T., 1996. Current developments and future research in catalytic membrane reactors. Membrane Sci. Tech. 4, 529-568.

10. Buxbaum, R. E., Kinney, A. B., 1996. Hydrogen Transport through Tubular Membranes of Palladium-Coated Tantalum and Niobium. Ind. Eng. Chem. Res. 35, 530-537.

11. Lin, Y. M., Rei, M. H., 2001. Study on the hydrogen production from methanol steam reforming in supported palladium membrane reactor. Catal. Today 67, 77-84.

12. Labinger, J. A., 1988. Oxidative coupling of methane: An inherent limit to selectivity? Catal. Lett. 1, 371-375.

13. Mortazavi, Y., Hudgins, R. R., Silveston, P. L., 1996. Catalytic methane coupling under periodic operation. Can. J. Chem. Eng. 74, 683-694.

14. Coronas, J., Gonzalo, A., Lafarga D., Menendaz, M. 1997. Effect of the membrane activity on the performance of a catalytic membrane reactor. AIChE J. 43, 3095-3104.

15. RIPI-NIOC, Document No. 18745-4163, Iran, 2004.

16. Stansch, Z., Mleczko, L., Baerns, M., 1997. Comprehensive Kinetics of Oxidative Coupling of Methane over the La_2O_3/CaO Catalyst. Ind. Eng. Chem. Res. 36, 2568-2579.

17. Montazer-Rahmati, M. M., Bargah-Soleimani, M., 2001. Rate equations for the Fischer-Tropsch reaction on a promoted iron catalyst. Can. J. Chem. Eng., 79, 800-804.

18. Rezaie, N., Jahanmiri, A., Moghtaderi, B., Rahimpour, M. R., 2005. A comparison of homogeneous and heterogeneous dynamic models for industrial methanol reactors in the presence of catalyst deactivation. Chem. Eng. Process. 44, 911-921.

19. Barbieri, G., Maio, F. P. D., 1997. Simulation of the Methane Steam Re-forming Process in a Catalytic Pd-Membrane Reactor. Ind. Eng. Chem. Res. 36, 2121-2127.

20. Shu, G., Grandjean, B. P. A., Kaliaguine, S., 1994. Methane steam reforming in asymmetric Pd- and Pd-Ag/porous SS membrane reactors. Appl. Catal. A.: Gen. 119, 305-325.

21. Hedden, J. A., 2000. Am. Chem. Soc. Div. Pet. Chem. 45, 202-210.

22. Kuntze, T., Hedden. K., Jess, A., 1995. Erdöl Erdgas Kohle 111, 67-71.

Figure Captions

Fig 1. Schematic diagram of two consecutive reactors: OCM and FT reactors.

Fig 2. (a) Schematic of two consecutive reactors: OCM and membrane FT reactors (b) detailed membrane FT reactor in co-current flow mode.

Fig 3. (a) Schematic of two consecutive reactors: OCM and membrane FT reactors (b) detailed membrane FT reactor in counter-current flow mode.

Fig 4. Variation of H_2/CO ratio that produced in OCM reactor as a function of CH_4/O_2 ratio (T = 1103 K, N_2 mole fraction = 0.337).

Fig 5. Effect of CH_4/O_2 ratio in OCM reactor feed on (a) CO conversion and (b) H_2 conversion (b) in CR (conventional fixed bed), CO-MR (co-current fixed bed membrane) and COUN-MR (counter-current fixed bed membrane) FT reactor (T = 1103 K, N_2 mole fraction = 0.337).

Fig 6. (a) Hydrogen partial pressure and (b) hydrogen injection rate as a function of FT Reactor in CO-MR and COUN-MR (T = 1103 K, N_2 mole fraction = 0.337).

Fig 7. Effect of CH_4/O_2 ratio in OCM reactor feed on (a) C_2H_4 yield and (b) C_2H_6 yield(b) in OCM reactor and CR, CO-MR, COUN-MR FT reactor (T = 1103 K, N_2 mole fraction = 0.337).

Fig 8. Effect of CH_4/O_2 ratio in OCM reactor feed on C_{5+} yield in CR, CO-MR and COUN-MR modes of FT reactor (T = 1103 K, N_2 mole fraction = 0.337).

Fig 9. Effect of CH_4/O_2 ratio in OCM reactor feed on (a) CH_4 yield and (b) CO_2 yield in CR, CO-MR and COUN-MR FT reactor (T = 1103 K, N_2 mole fraction = 0.337).

Fig 10. Variation of H_2/CO ratio that produced in OCM reactor as a function of N_2 % in feed of OCM reactor (CH_4/O_2 = 12, T = 1103 K).

Fig 11. Effect of N_2 % in OCM reactor feed on (a) CO conversion and (b) H_2 conversion in CR, CO-MR and COUN-MR FT reactor (CH_4/O_2 = 12, T = 1103 K).

Fig 12. variation of (a) C_2H_4 yield and (b) C_2H_6 yield in CR, CO-MR, COUN-MR FT reactor and OCM reactor as a function of N_2 % in OCM reactor feed (CH_4/O_2 = 12, T = 1103 K).

Fig 13. variation of C_{5+} yield in CR, CO-MR and COUN-MR FT reactor as a function of N_2 % in OCM reactor feed (CH_4/O_2 = 12, T = 1103 K).

Fig 14. Effect of N_2 % in OCM reactor feed on (a) CH_4 yield and (b) CO_2 yield in CR, CO-MR and COUN-MR FT reactor (CH_4/O_2 = 12, T = 1103 K).

Fig 15. CO mole flow vs. length of reactor in OCM and FT reactor in CR, CO-MR and COUN-MR modes (CH_4/O_2 = 12, T = 1103 K).

Fig 16. H_2 mole flow vs. length of reactor in OCM and three modes of operation of FT reactor.

Fig 17. Variation of C_2H_4 mole flow (a) in OCM and FT reactor (in CR, CO-MR and COUN-MR modes) along CR, CO-MR and COUN-MR FT reactor (CH_4/O_2 = 12, T = 1103 K).

Fig 18. Variation of C_2H_6 mole flow in OCM and FT reactor (in CR, CO-MR and COUN-MR modes) (CH_4/O_2 = 12, T = 1103 K).

Fig 19. Variation of (a) C_3H_8 mole flow and (b) C_3H_8 yield in FT reactor in CR, CO-MR and COUN-MR (CH_4/O_2 = 12, T = 1103 K).

Fig 20. Variation of (a) C_{5+} mole flow and (b) C_{5+} yield in FT reactor in CR, CO-MR and COUN-MR FT reactor (CH_4/O_2 = 12, T = 1103 K).

Fig 21. Variation of (a) i-C_4H_{10} mole flow and (b) i-C_4H_{10} yield in FT reactor in CR, CO-MR and COUN-MR FT reactor (CH_4/O_2 = 12, T = 1103 K).

Fig 22. Variation of (a) n-C_4H_{10} mole flow and (b) n-C_4H_{10} yield in CR, CO-MR and COUN-MR FT reactor (CH_4/O_2 = 12, T = 1103 K).

Fig 23. Variation of (a) CO_2 yield and (b) CH_4 yield in CR, CO-MR and COUN-MR FT reactor (CH_4/O_2 = 12, T = 1103 K).

Fig 24. C_{5+} yield vs. (a) CH_4/O_2 ratio, (b) N_2% in OCM reactor feed and (c) length of FT reactor.

Fig 25. Gas phase temperature vs. length of reactor in (a) OCM reactor (b) in CR, CO-MR and COUN-MR FT reactor (CH_4/O_2 = 12).

Fig 26. (a) variation of H_2/CO ratio vs. contact time in OCM reactor (b) variation of C_{5+} yield vs. contact time in CR, CO-MR and COUN-MR FT reactor (CH_4/O_2 = 12, T = 1103 K).

List of Tables

Table 1 FTS pilot plant characteristics [15].

Parameter	Value
Tube dimension (mm)	Ø38.1×3×12 000
Feed temperature (K)	569
Cooling temperature (K)	566.2
Reactor pressure (kPa)	1700
Catalyst density (kgm^{-3})	1290
Catalyst sizes (mm)	Ø2.51×5.2
Bulk density (kgm^{-3})	730
Tube length (m)	12
Number of tubes	1
GHSV (h^{-1})	235
Feed molar flow rate ($gmol\ s^{-1}$)	0.0335
Bed voidage	0.488

Table 2 OCM Reactor parameters and constants

Parameter	Dimension
Inner diameter (mm)	38.1
Pressure (kPa)	110
Length of catalyst bed (mm)	12000
Catalyst weight, m_{cat} (g)	0.007 - 1.000
Flow rate (STP), υ_{STP} ($m^3\ s^{-1}$)	4×10^{-6} - 13×10^{-4}
Catalyst size (mm)	0.25 - 0.35
Catalyst density (kgm^{-3})	3600

Table 3 Catalyst and specifications of membrane FT system.

Parameter	Value
Tube dimension (mm)	Ø38.1×3×12 000
Inner radius of Pd-Ag layer (mm)	19.05
outer radius of Pd-Ag layer (mm)	19.065
Reactor radius (mm)	27
Feed temperature (K)	565
Cooling temperature (K)	555
Reactor inlet pressure (kPa)	1700

Catalyst density (kgm^{-3})	1290
Catalyst equivalent diameter (m)	3.83×10^{-3}
Bulk density (kgm^{-3})	730
Tube length (m)	12
Number of tubes	1
GHSV (h^{-1})	235
Feed molar flow rate ($gmol\ s^{-1}$)	0.0335
Catalyst thermal conductivity ($kJm^{-1}s^{-1}k^{-1}$)	0.00625
Bed voidage	0.488

Table 4 kinetic parameters of OCM reactions [16].

Step	$k_{0,j}$ ($mol\ g^{-1}\ s^{-1}\ pa^{-(m+n)}$)	$E_{a,j}$ ($kJ\ mol^{-1}$)	m_j	n_j	K_{j,co_2} (pa^{-1})	$\Delta H_{ad,co_2}$ ($kJ\ mol^{-1}$)	K_{j,o_2} (pa^{-1})	$\Delta H_{ad,o_2}$ ($kJ\ mol^{-1}$)
1	0.2×10^{-5}	48	0.24	0.76	0.25×10^{-12}	-175		
2	23.2	182	1.0	0.40	0.83×10^{-13}	-186		
3	0.52×10^{-6}	68	0.57	0.85	0.36×10^{-13}	-187	0.23×10^{-11}	-124
4	0.11×10^{-3}	104	1.0	0.55	0.40×10^{-12}	-168		
5	0.17	157	0.95	0.37	0.45×10^{-12}	-166		
6	0.06	166	1.0	0.96	0.16×10^{-12}	-211		
7	1.2×10^{7}[a]	226						
8	9.3×10^{3}	300	0.97	0				
9	0.19×10^{-3}	173	1.0	1.0				
10	0.26×10^{-1}	220	1.0	1.0				

[a]Units are $mol\ s^{-1}\ m^{-3}\ pa^{-1}$

Table 5 Kinetic parameter data of Fischer-Tropsch synthesis [17].

Reaction no.	m	n	K_i	E_i
1	-1.0889	1.5662	142583.8	83423.9
2	0.7622	0.0728	51.556	65018
3	-0.5645	1.3155	24.717	49782
4	0.4051	0.6635	0.4632	34885.5
5	0.4728	1.1389	0.00474	27728.9
6	0.8204	0.5026	0.00832	25730.1
7	0.5850	0.5982	0.02316	23564.3
8	0.5742	0.710	410.667	58826.3

Table 6 Comparison between experimental and simulated data.

	1023 K	1073 K	1103 K	973 K	1023 K	1103 K
Feed mole fraction						
CH_4	0.612	0.612	0.612	0.699	0.699	0.699
O_2	0.051	0.051	0.051	0.095	0.095	0.095
N_2	0.337	0.337	0.337	0.206	0.206	0.206
CH_4 conversion (%)						
Experimental	4.9	7.9	9.9	4.1	7.1	14.4
Simulated	4.73	8.41	10.8	3.15	6.18	14.45
Error (%)	3.47%	6.46%	9.1%	23.17%	1.13%	0.35%
C2 selectivity (%)						
Experimental	55.6	69.2	72.5	35.6	53.7	69.6
Simulated	57.25	64.99	65.21	38.41	50.98	59.75
Error (%)	2.97%	6.08%	10.06%	7.89%	5.07%	14.15%
C2 yield (%)						
Experimental	2.7	5.5	7.2	1.5	3.8	10
Simulated	2.7	5.5	7.4	1.21	3.15	8.63
Error (%)	0%	0%	2.78%	19.3%	17.11%	13.7%

Table 7 Comparison between CR model results with pilot plant data for fresh catalyst.

Parameter	Pilot plant data	Calculated	Error (%)
X_{CO} (%)	77.94	77.19	0.96%
X_{H_2} (%)	92.83	94.5	1.8%
C5 selectivity	42.55	45.64	7.3%
CO_2 selectivity	339.07	317.32	6.4%
CH_4 selectivity	44.15	44.65	1.1%
H_2O selectivity	120.67	115.19	4.5%
C_2H_4 selectivity	3.95	3.52	1.1%
C_2H_6 selectivity	11.78	13.93	18.25%
n-C_4 selectivity	11.07	9.65	12.82%
i-C_4 selectivity	14.45	12.23	15.36%
C_3H_8 selectivity	9.33	6.42	31.19%

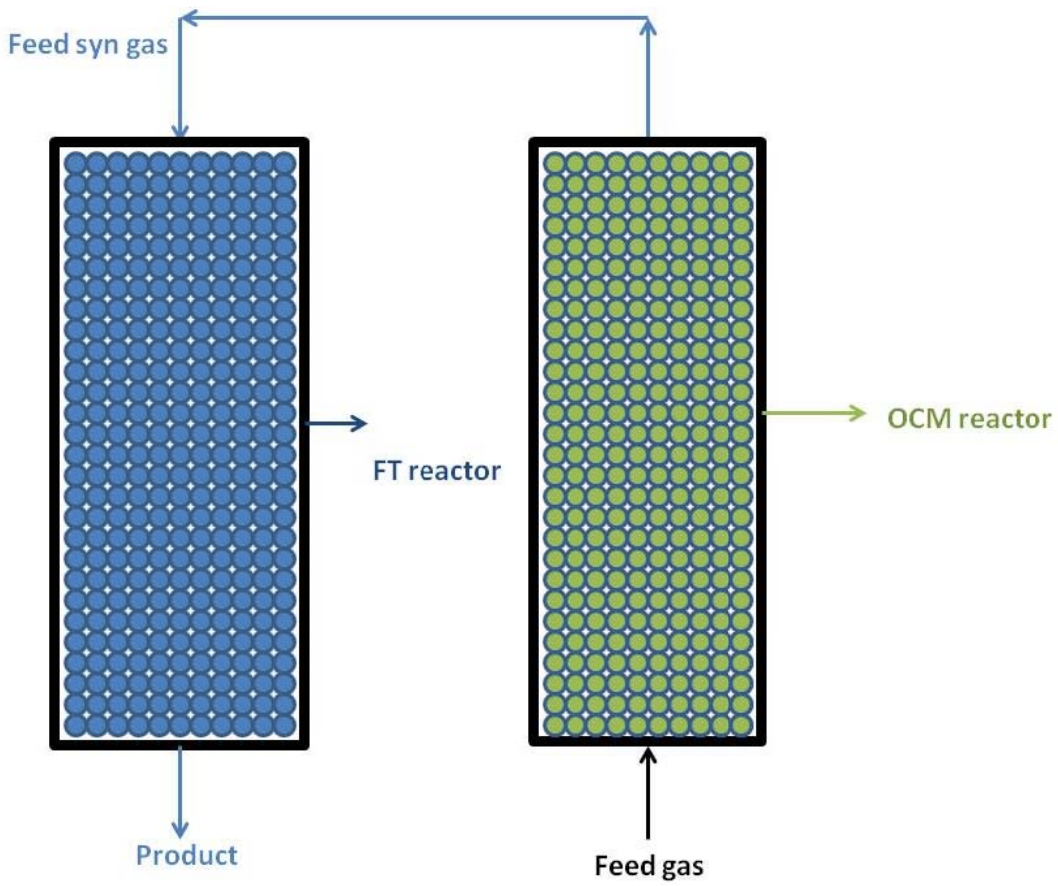

Fig. 1

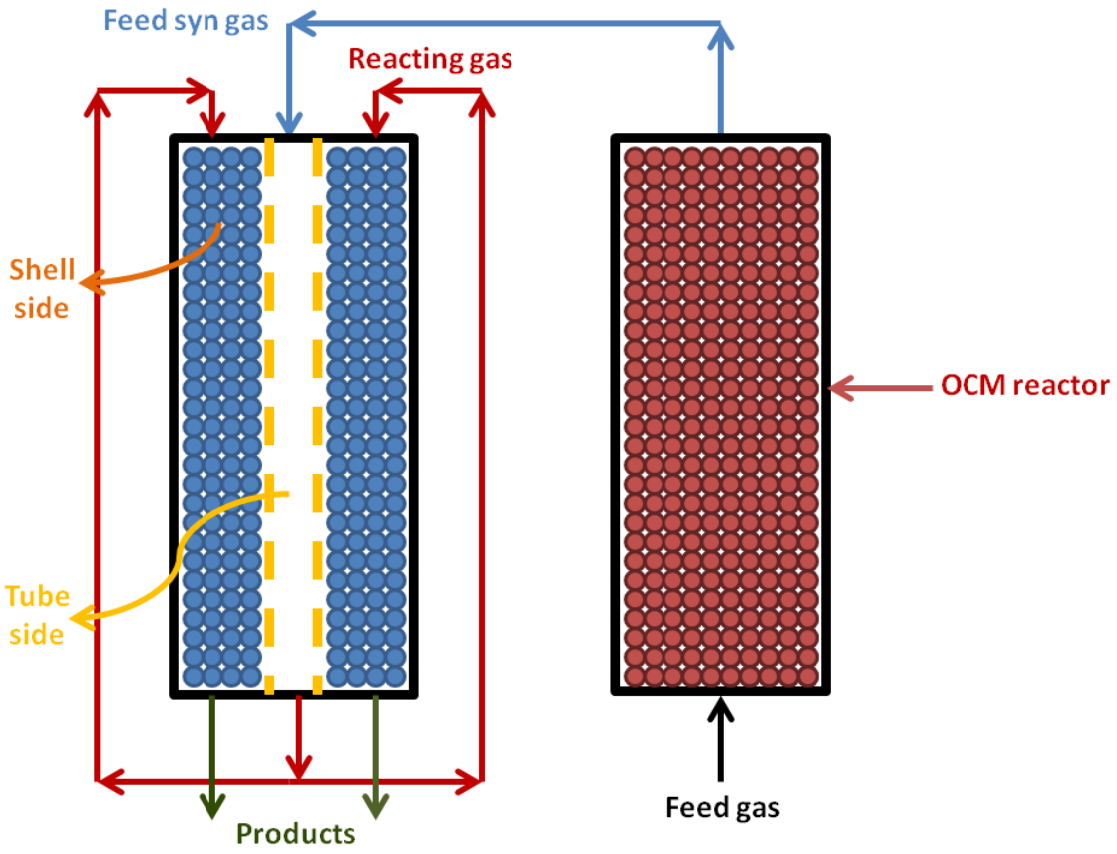
Feed syn gas
Reacting gas
Shell side
Tube side
OCM reactor
Products
Feed gas

Fig. 2(a)

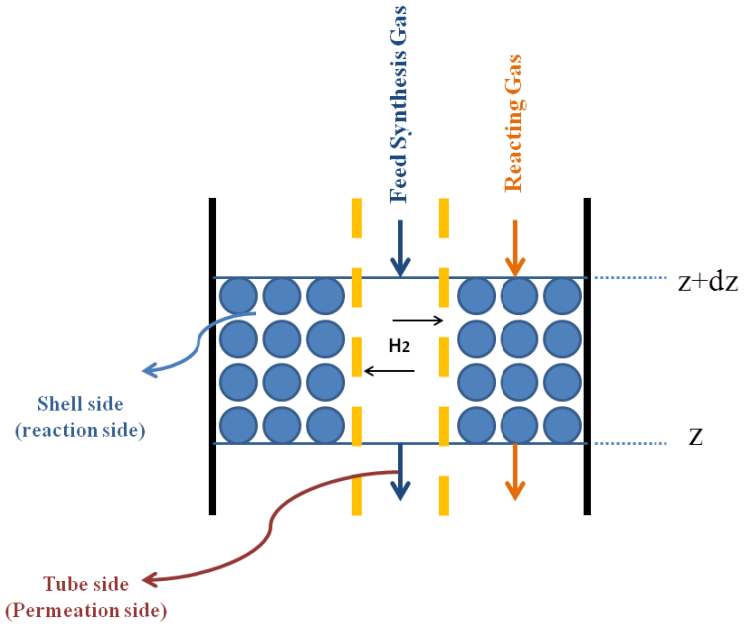
Feed Synthesis Gas
Reacting Gas
z+dz
H2
Shell side
(reaction side)
z
Tube side
(Permeation side)

Fig. 2(b)

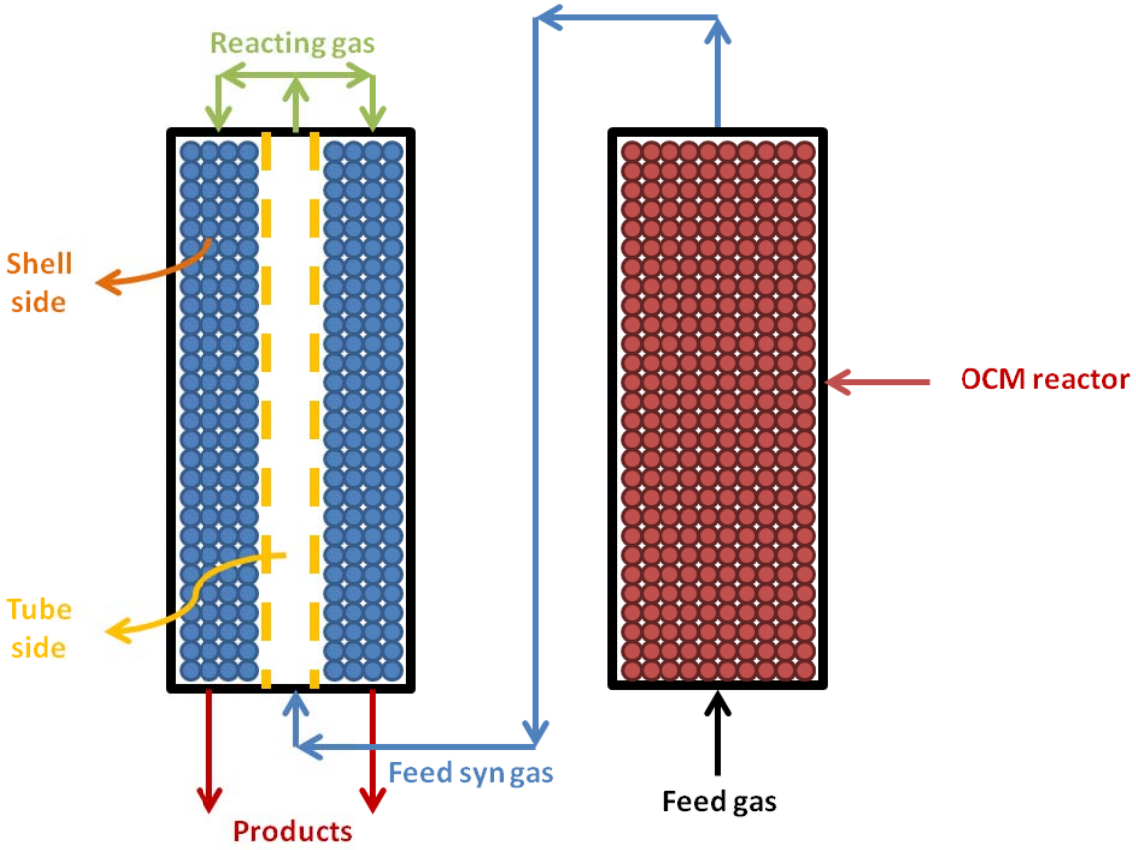
Reacting gas
Shell side
Tube side
OCM reactor
Feed syn gas
Products
Feed gas

Fig. 3(a)

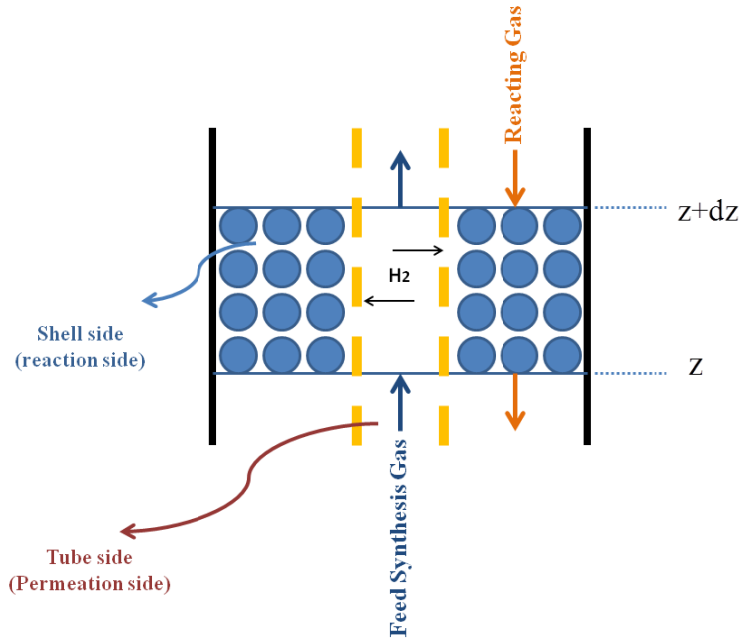
Reacting Gas
z+dz
H2
Shell side
(reaction side)
z
Feed Synthesis Gas
Tube side
(Permeation side)

Fig. 3(b)

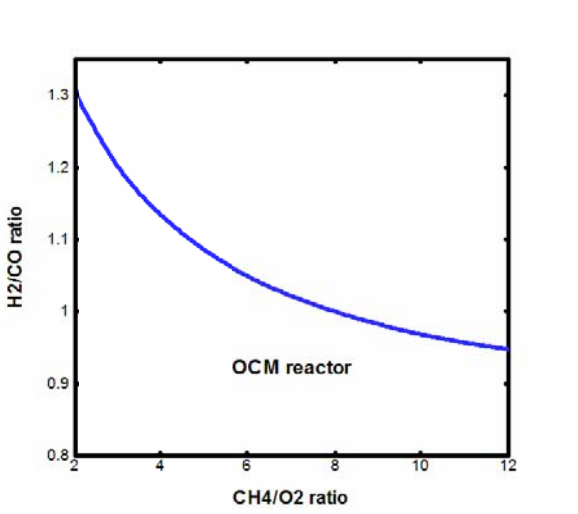

Fig. 4

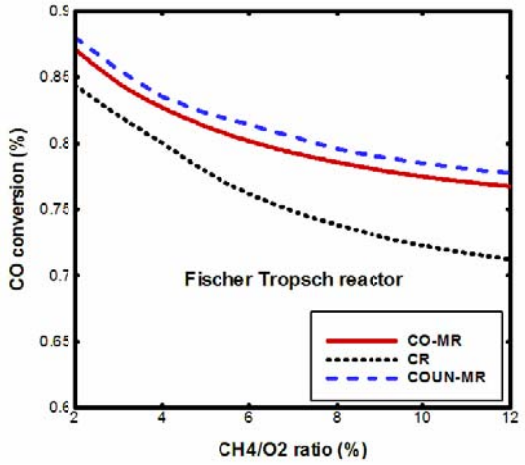

Fig. 5(a)

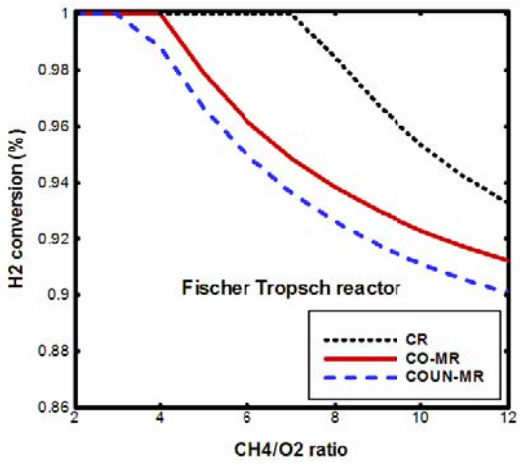

Fig. 5(b)

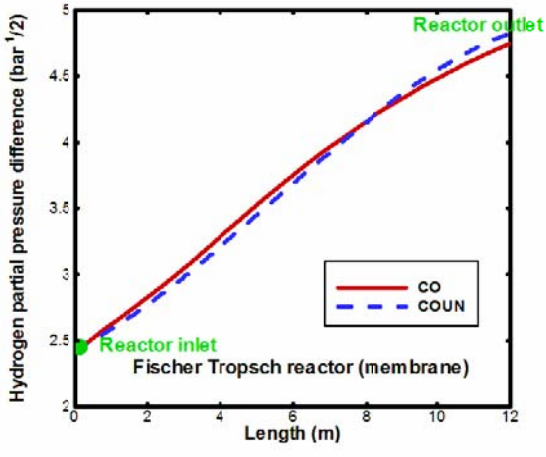

Fig. 6(a)

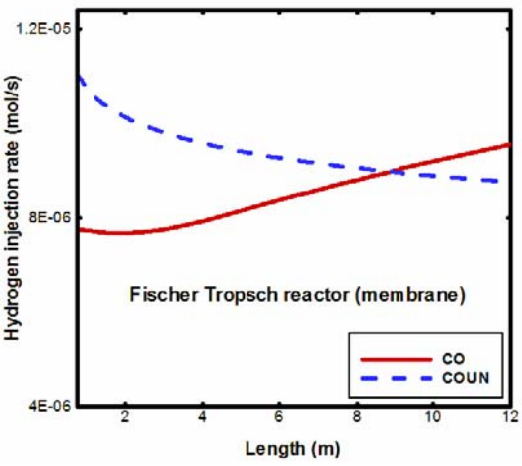

Fig. 6(b)

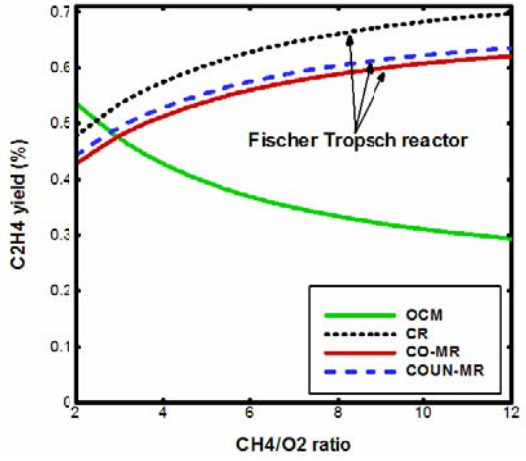

Fig. 7(a)

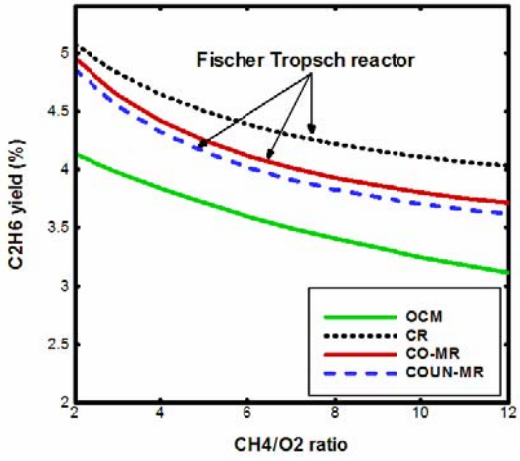

Fig. 7(b)

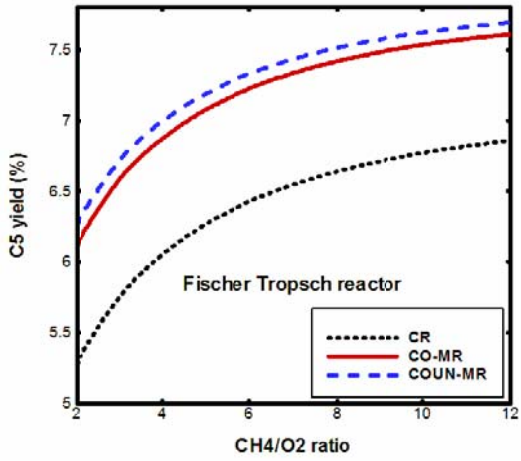

Fig. 8

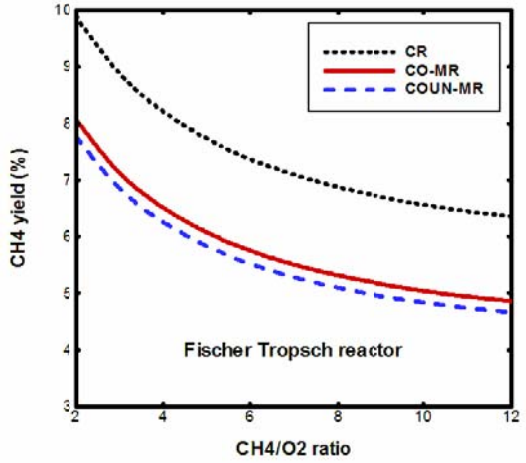

Fig. 9(a)

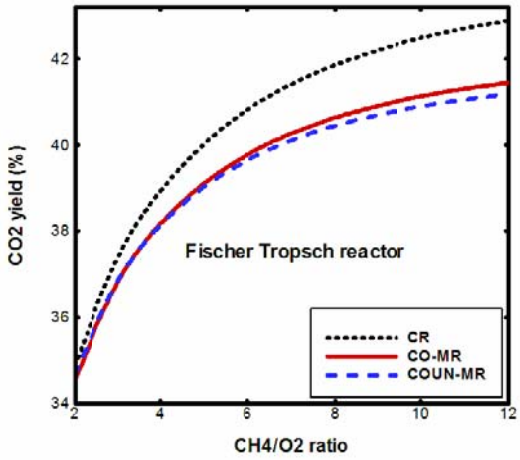

Fig. 9(b)

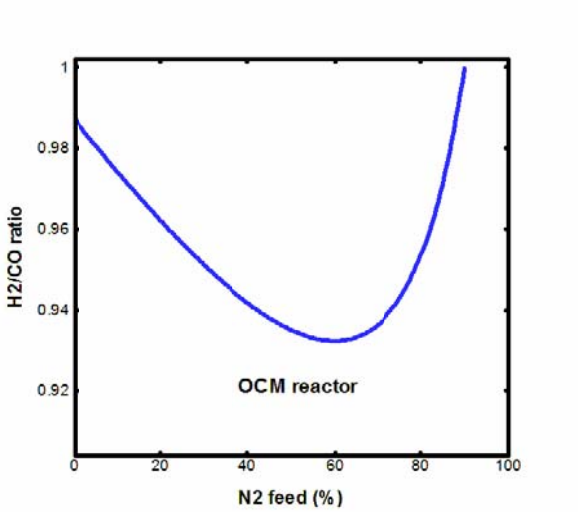

Fig. 10

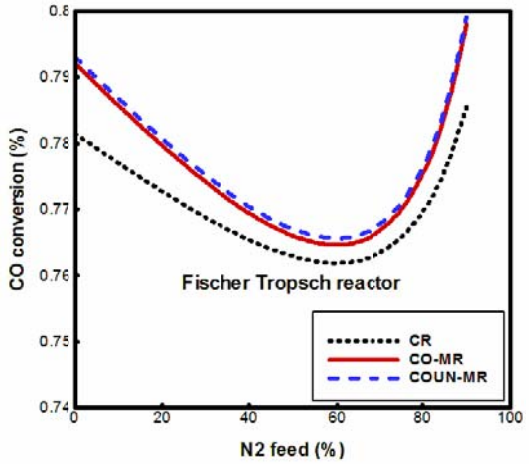

Fig. 11(a)

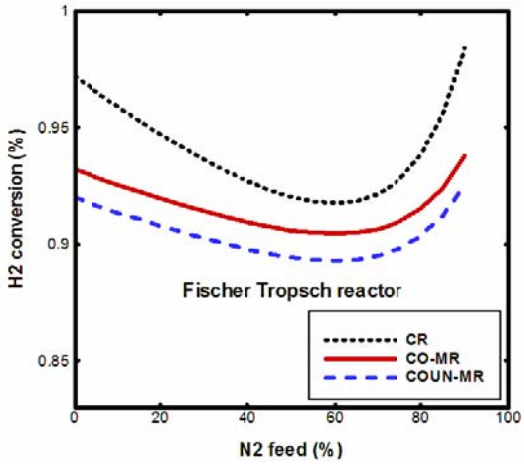

Fig. 11(b)

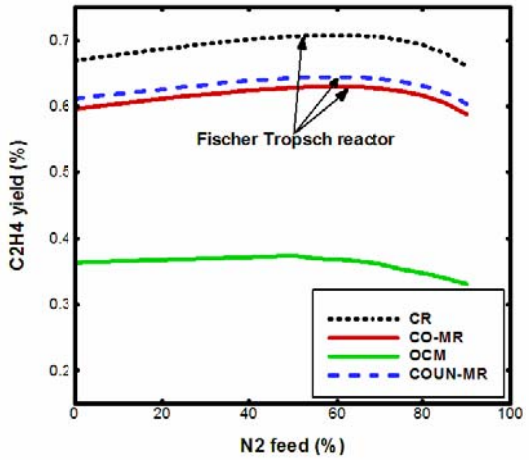

Fig. 12(a)

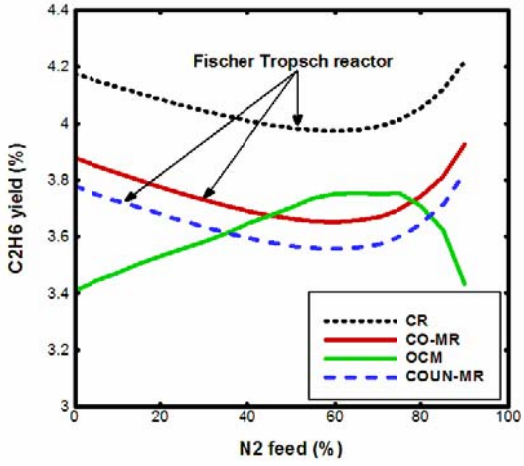

Fig. 12(b)

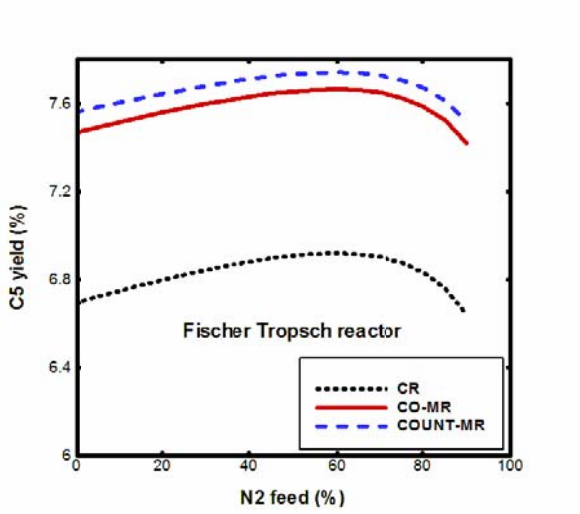

Fig. 13

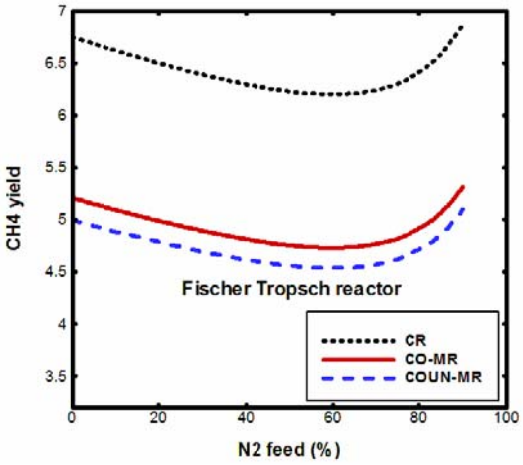

Fig. 14(a)

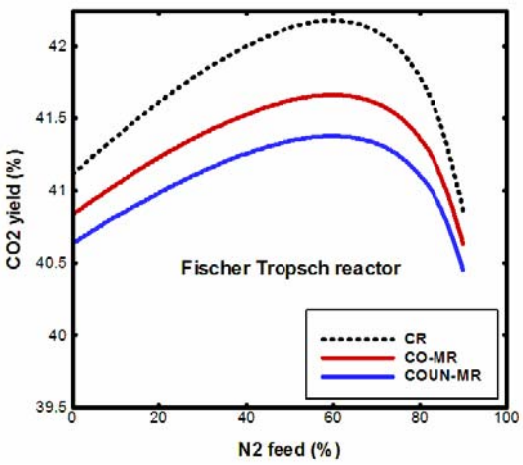

Fig. 14(b)

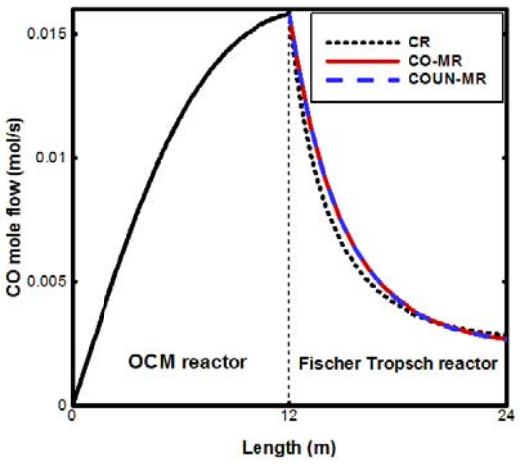

Fig. 15(a)

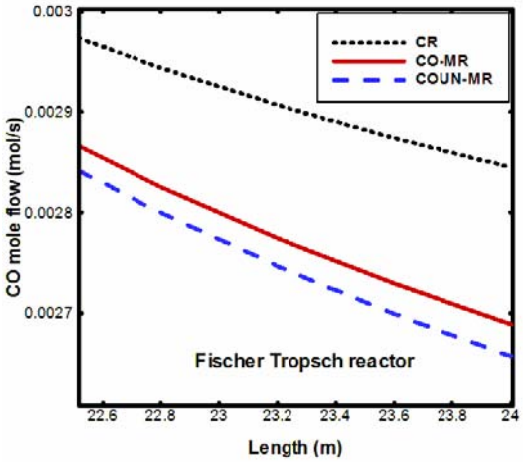

Fig. 15(b)

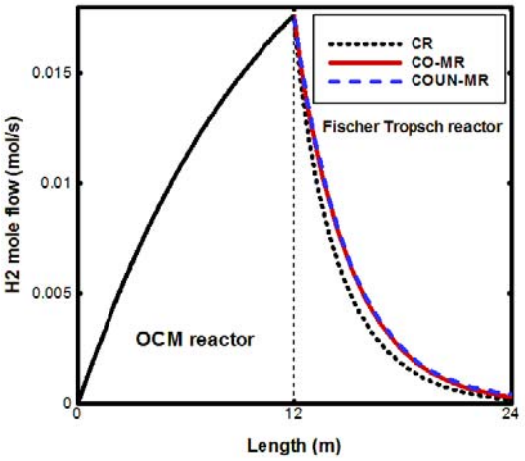

Fig. 16(a)

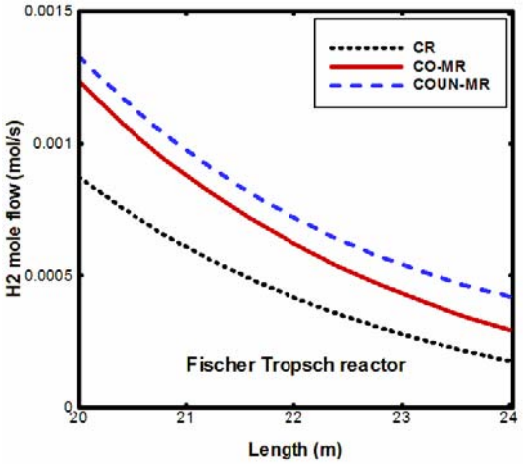

Fig. 16(b)

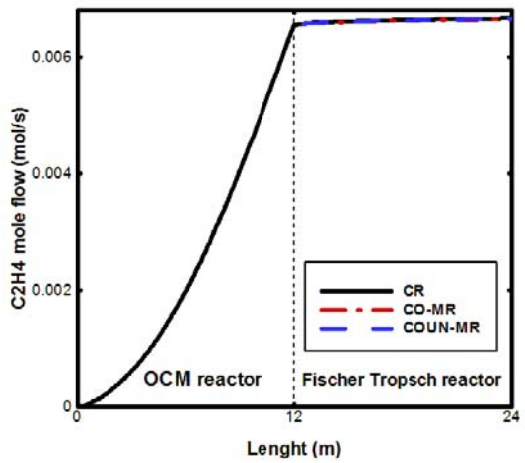

Fig. 17(a)

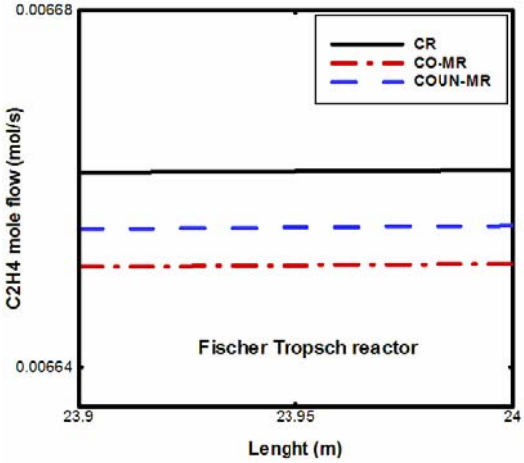

Fig. 17(b)

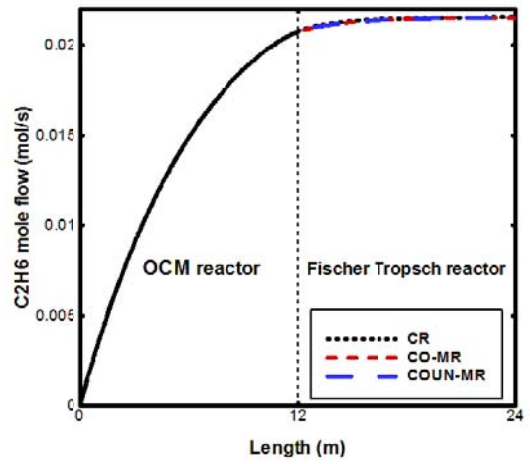

Fig. 18(a)

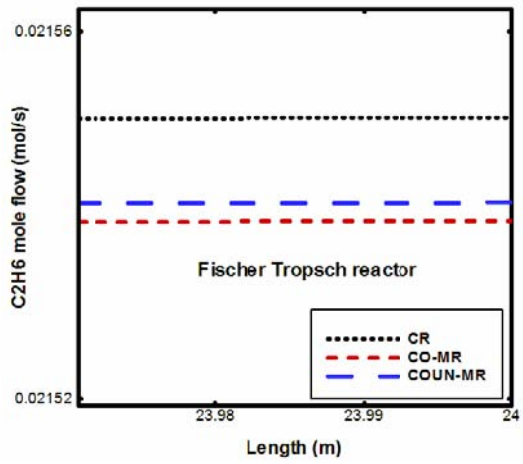

Fig. 18(b)

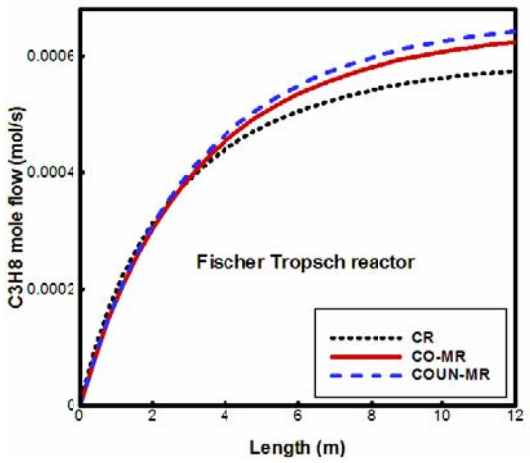

Fig. 19(a)

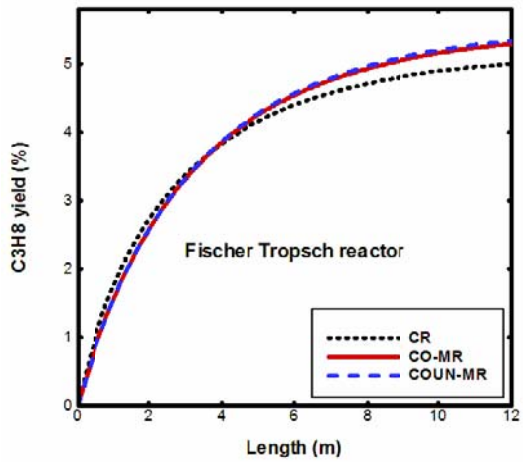

Fig. 19(b)

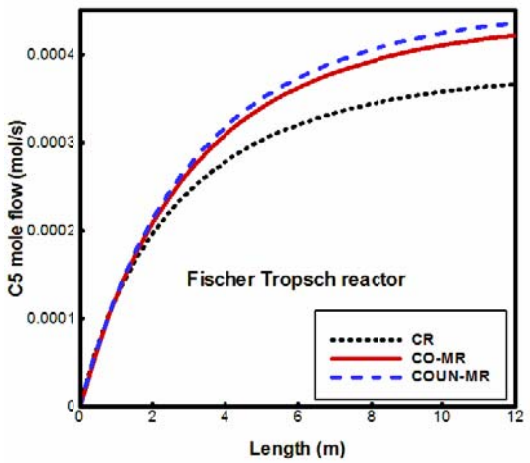

Fig. 20(a)

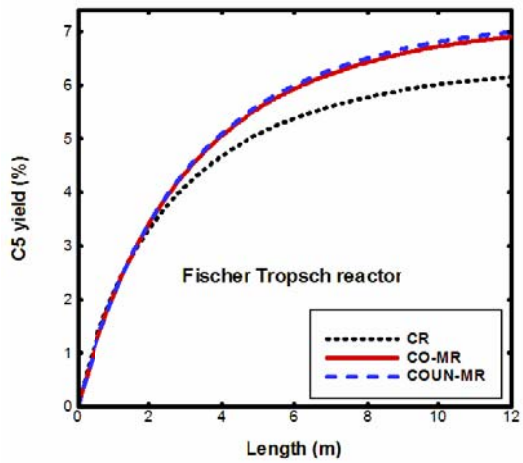

Fig. 20(b)

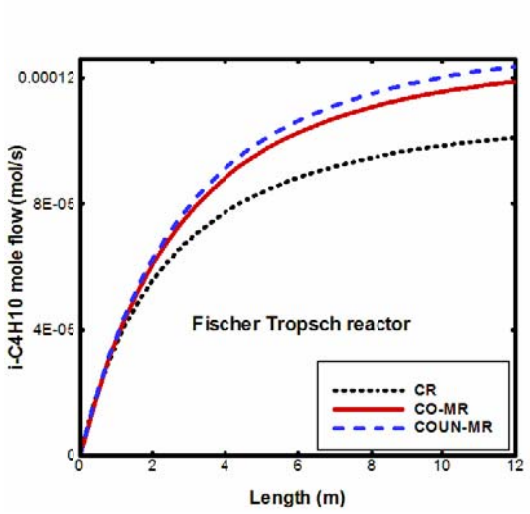

Fig. 21(a)

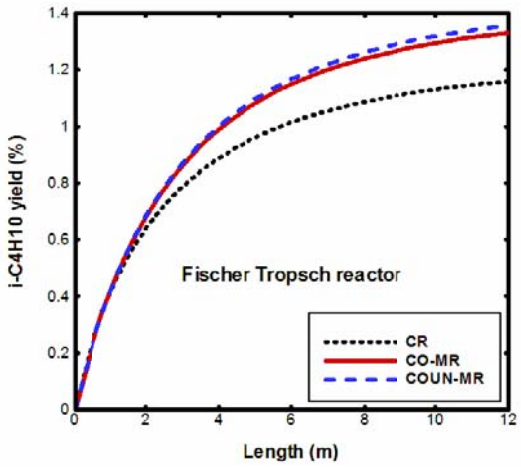

Fig. 21(b)

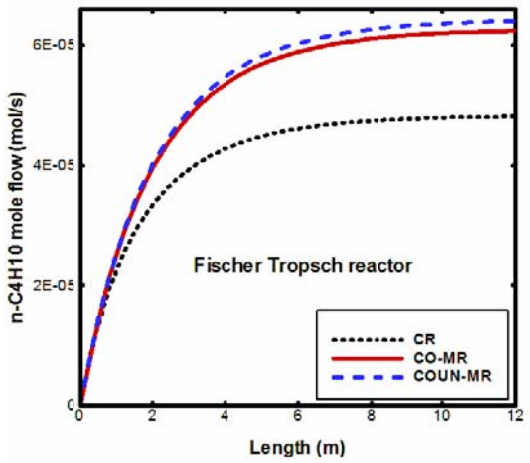

Fig. 22(a)

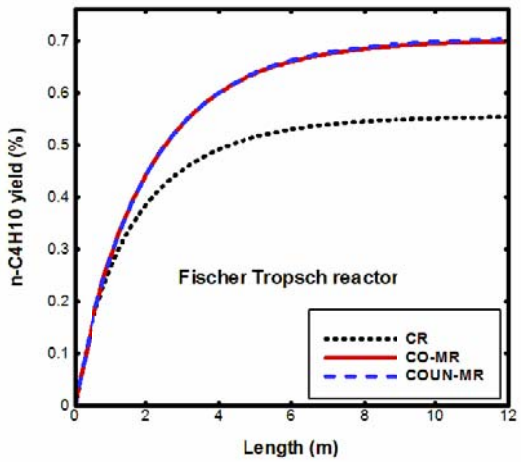

Fig. 22(b)

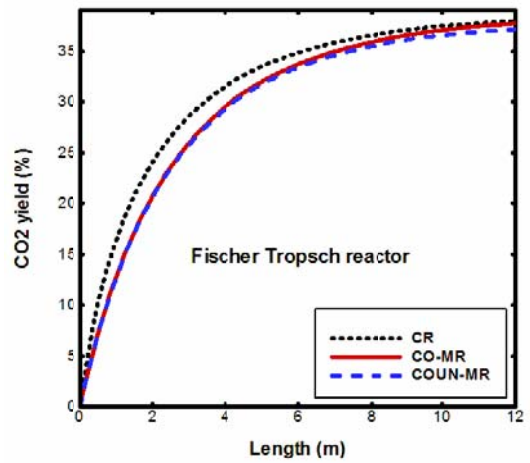

Fig. 23(a)

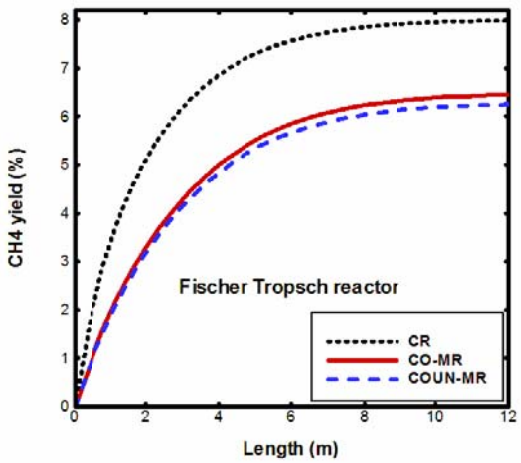

Fig. 23(b)

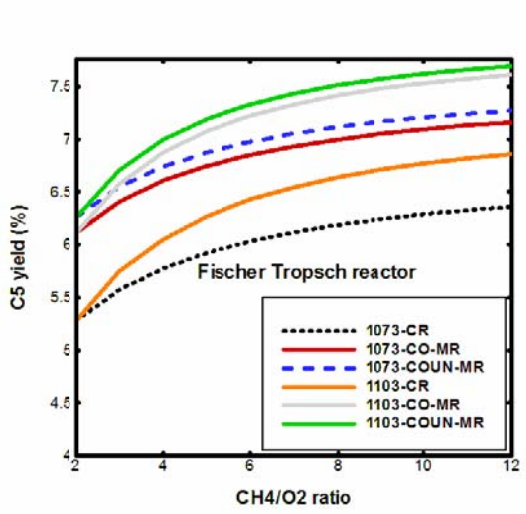

Fig. 24(a)

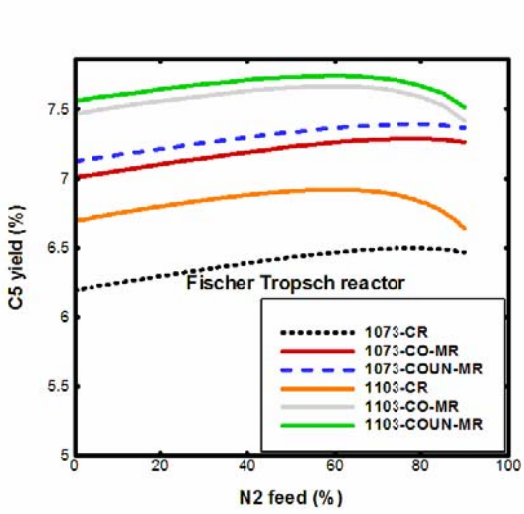

Fig. 24(b)

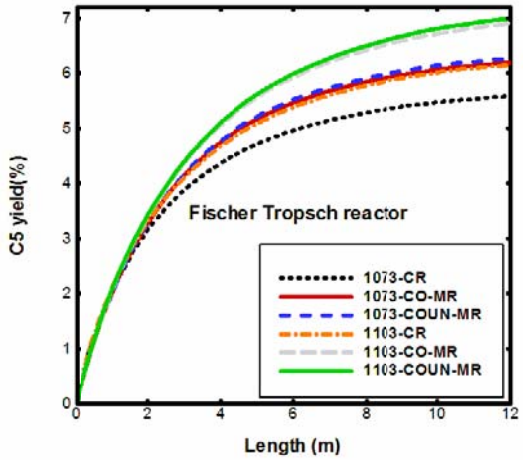

Fig. 24(c)

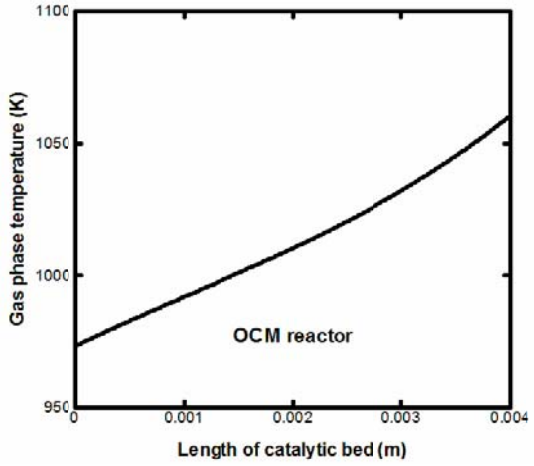

Fig. 25(a)

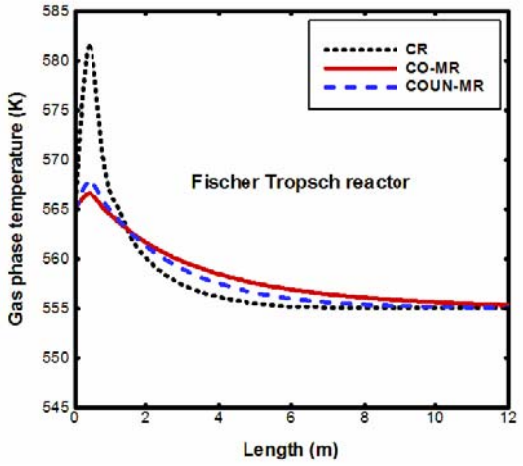

Fig. 25(b)

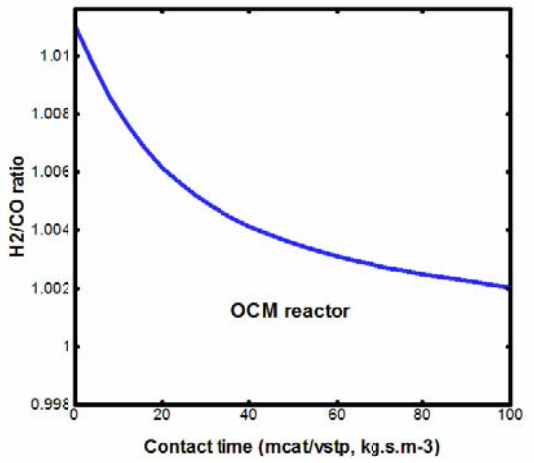

Fig. 26(a)

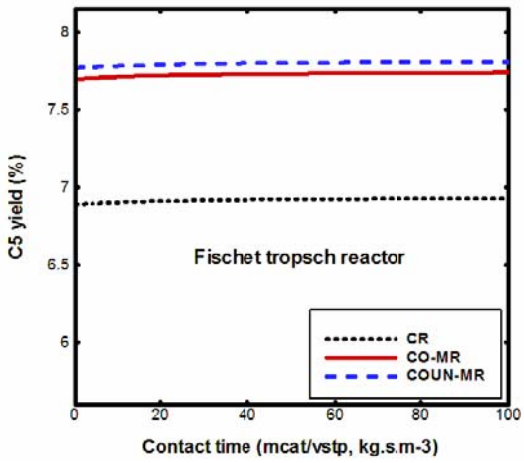

Fig. 26(b)